



Fragmentation of an armour piercing projectile after impact on composite covered alumina tiles



D.B. Rahbek*, B.B. Johnsen

Norwegian Defence Research Establishment (FFI), P.O. Box 25, NO-2027 Kjeller, Norway

ARTICLE INFO

Keywords:

Alumina ceramic
Composite cover
Ballistic testing
Armour piercing projectile
Core fragmentation

ABSTRACT

In a typical body armour system, a hard armour plate is often used in conjunction with a soft ballistic panel. The main purpose of the armour plate is to erode and fragment an impacting projectile, such as 7.62 mm armour piercing (AP) projectiles with a very hard material core. This is made possible by employing a single ceramic tile as the strike face. This tile is covered by a sheet material. The sheet cover may improve the ballistic performance by partly maintaining the integrity of the ceramic. In this study, the effect of adding a composite cover has been investigated experimentally by ballistic testing of different types of composite-covered targets. The targets were totally perforated by a 7.62 mm AP hard steel core projectile at near-muzzle velocities (around 800 m/s). The post-impact process was monitored by high speed video, and the resulting core fragments were collected and analysed. This allowed the core fragmentation, residual velocity and kinetic energy-loss to be quantified. The results showed that the core fragmentation and the kinetic energy-loss of the projectile were most significant for the targets with the composite-cover on the back of the alumina. For targets with four composite back-layers, and an increased areal density of 9.5%, the mass of the projectile core was reduced by 61%, while the kinetic energy was reduced by 84%. The residual velocity did not vary to the same extent between the different target configurations. The mechanism behind the positive effect of a back cover is believed to be delayed opening of tensile cracks that originate from the back of the ceramic, which gives more time for interaction with the penetrator.

1. Introduction

Ceramics are commonly used in combination with other materials for ballistic protection of civilian and military equipment where low weight is a key requirement [1–3]. This may be vehicles, aircraft, personnel, or any other application where mobility is important. Ceramics are attractive materials because they offer low density and high hardness. This promotes their use in light-weight ballistic protection systems, where their role is to erode, blunt and shatter the projectile. Tiles of various size and thickness are employed, depending on the application. However, one inherent property of ceramics is their brittleness, and they will fracture in a brittle manner when subjected to high stress loads (particularly tensile loads). When impacted by a projectile, the ceramic can fail by different modes depending on the projectile material, size and shape, and the ceramic properties and size/thickness. In front of the penetrator, micro-cracking and lattice plasticity can occur in the ceramic, while radial and cone cracking extend further out in the ceramic tile [4–9]. Upon formation of cone and radial cracks in the ceramic, the tile breaks in pieces and the comminuted/

crushed ceramic in front of the penetrator becomes less confined in the projectile path, which results in lower penetration resistance. This is an important issue that needs to be considered when designing an armour system, and it is usually solved by combining the ceramic with other materials.

One important application of ceramics is found for body armour. The introduction of body armour has resulted in a reduction of the thoracic injuries for military combatants [10], i.e. the number of casualties in recent military conflicts has been reduced by the use of body armour. A typical body armour system consists of a soft ballistic panel and a hard armour plate. In a military context, the main purpose of the soft panel, usually made from aramid and/or ultra-high molecular weight polyethylene (UHMWPE), is to protect against fragments from various types of explosions, while the main purpose of the armour plate is to protect against rifle threats, such as hard core armour piercing (AP) projectiles.

In hard armour plates, the strike face is made up of a single ceramic tile which is typically alumina, silicon carbide or boron carbide, and backed with several layers of ballistic fibres. The ceramic tile is often

* Corresponding author.

E-mail address: dennis-bo.rahbek@ffi.no (D.B. Rahbek).

covered by a sheet material to improve the ballistic performance, usually a fibre composite material [11]. When the ceramic is covered by a sheet material, the ceramic will be partly held together both during and after a projectile impact. The fractured ceramic is then prevented from moving and held in place in the path of the penetrator. This gives more time for erosion and fragmentation of the projectile. It was also pointed out by Horsfall and Buckley [12] that a single laminate polymer composite spall shield on the front of the ceramic will act to confine the ceramic tile. This contributes to improved multi-hit performance, since the spall shield introduces radial constraint on the ceramic surface, which then prevents through-thickness cracks from opening and confines larger ceramic fragments that are formed during impact. The effect of through-thickness cracks on multiple hits is then reduced.

Many hard armour plates are designed to protect against AP projectiles with caliber up to 7.62 mm. These AP projectiles contain a core that is made of a hard material, either a steel with high carbon and/or high alloy element content, or a non-ferrous, high density material (e.g. tungsten heavy alloy (WHA), tungsten carbide) [13]. When the projectile impacts on the armour at a given velocity it is desirable, from a protection point of view, that the core material of the projectile is eroded and fragmented as much as possible, and that the core fragments are slowed down considerably, thus reducing the kinetic energy. In this respect, it is the largest projectile fragment that is the most critical, since it will have the highest kinetic energy and, hence, the highest probability of perforation.

New designs of composite-covered ceramics are continuously sought to improve penetration resistance and to ultimately enhance personal protection. Several studies have looked into how the failure of the ceramic tiles is affected by a composite cover (or other sheet materials) [14–20]. Some of the studies were performed using regular and AP projectiles, but also other projectile geometries, such as spherical and cylindrical, have been employed. The impact velocities in the referenced studies ranged from around 200 m/s to 900 m/s. In all the studies, the target design (e.g. the ceramic, sheet material, number of layers, etc.) and the experimental conditions (e.g. type of projectile, impact velocity, ballistic test procedure, etc.) were different. Hence, the studies do not fully agree on how the ballistic performance changes with addition of a composite cover to a ceramic tile. Few studies have tried to isolate the effects of front and back covers, since the composite layer was usually present on both sides, or the composite was wrapped around the tile. Nevertheless, Sarva et al. [14] found significant effects from adding a front cover to the ceramic, but little extra effect from an additional back cover. One proposed mechanism which contributed to the increased performance of the front-covered ceramic is the constraining effect on the ceramic debris on the front. This constraint increases the flow of ceramic debris towards the penetrator, gives more time for penetrator-ceramic interaction, since the ceramic is kept in front of the penetrator for a longer period of time, and slows down propagation of cracks in the ceramic [14–16]. If these effects can be utilized, hard armour plates with a lower areal density can be produced.

It is clear from the references in the previous paragraph, that adding a front composite cover-layer of high-strength fibres to the ceramic, in the form of unidirectional sheets or woven fabrics, can improve the ballistic performance. This is investigated further in the present paper, where ballistic experiments on bare and composite-covered (on front and/or back) alumina tiles are described. A glass fibre-reinforced composite was used for covering the tiles. Different target configurations where the composite cover was placed on the front and/or the backside of the alumina tiles were tested. To our knowledge, this is the first study that in a systematic way tries to isolate the effects of front and back covers. The main goal of the experiments was to investigate whether the composite cover contributes to higher erosion and fragmentation of the projectile. Therefore, in the ballistic experiments, the free-standing targets were totally perforated by a 7.62 mm AP hard steel core projectile at near-muzzle velocities (around 800 m/s). High speed filming was used to measure the residual velocity of the fragmented

projectile core, and the core fragments were collected and analysed. This allowed the size distribution of core fragments, and thereby the erosion and fragmentation of the core, to be quantified.

2. Experiments

2.1. Materials

The alumina (aluminium oxide, Al_2O_3) employed was Alotec 98 SB from CeramTec (Plochingen, Germany). The alumina content of the ceramic was 98%, with density 3.8 g/cm^3 , porosity $< 2\%$, medium grain size $6 \mu\text{m}$, Vickers hardness 13.5 GPa , and Young's modulus 335 GPa . The size of the alumina ceramic tiles was $100.1 \text{ mm} \times 100.1 \text{ mm} \times 8.2 \text{ mm}$, the mass 318 g , and the areal density 31.7 kg/m^2 .

The composite employed was glass fibre in a thermoplastic polyester (polyethylene terephthalate, PET) matrix, delivered by Comfil (Gjern, Denmark). A woven fabric of commingled glass fibres and PET fibres was employed. The fabric is a balanced twill 2/2. In this fabric, the crosswise yarns are carried over and under two lengthwise yarns in the weaving process, and each row of crosswise yarns is offset to create the twill 2/2 pattern. The thermoplastic polymer fibres form a consolidated matrix with low porosity content upon melting and cooling. For the consolidated composite material, the nominal fibre content was 57% by weight and 42% by volume, and the density was 1.87 g/cm^3 . The thickness and areal density of one composite layer were 0.4 mm and 0.75 kg/m^2 , respectively.

2.2. Target configurations

Targets for ballistic testing, where the alumina was covered with the composite material, were produced. In addition to the bare alumina tile, alumina/composite target configurations where two or four layers of the composite material covered the front and/or backside of the alumina were employed. Details about the different configurations that were produced and tested are given in Table 1. The increase in areal density when adding two and four composite layers to the alumina was 4.7% and 9.5%, respectively.

The alumina/composite targets were produced via a vacuum-assisted moulding process. A vacuum oven with a heated aluminium plate and a covering silicon bag was employed. The alumina was first cleaned by acetone degreasing. The correct number of fabric layers was then added to the front and/or the back of the alumina tile. Heating under vacuum was thereafter conducted at $215 \text{ }^\circ\text{C}$ for 75 min, which led to melting of the polymer, infiltration of the glass fibres, and the formation of a consolidated matrix upon cooling. The consolidated polyester matrix gave good adhesion between the alumina and the composite [21].




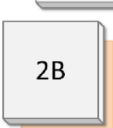
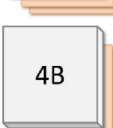
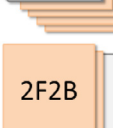
2.3. Ballistic testing

The projectile used for testing was a standard $7.62 \times 63 \text{ mm}$ M2 AP [24], shown in Fig. 1. The projectile has a 5.19 g armour piercing (AP) hardened steel core, a 0.7 g lead filler in front of the steel core, a 0.4 g copper cup, and a 4.4 g copper jacket [22]. The total mass of the projectiles used for the tests was on average $10.56 \pm 0.01 \text{ g}$ (\pm standard deviation).

A test barrel (1:12 twist, 562 mm bore length from Prototypa) was used to accelerate the projectile using cartridges loaded with gun powder. The test set-up is shown in Fig. 2. A laser velocity screen (VFR-2 from Prototypa) was used to measure the projectile velocity. The velocity screen was located 5.5 m from the from the gun barrel, while the target strike face was positioned at a distance of 11.5 m. The impact velocity at the target position was corrected for the effect of drag between the velocity screen and the target, and a correction factor of 0.73 m/s/m was employed [23,24]. The average impact velocity was

Table 1

List of tested targets. 2F designates a target with two layers of composite material on the front of the ceramic tile, 2B a target with two layers on the back of the ceramic tile, and 2F2B a target with two layers on each side of the ceramic tile.

Target type	Configuration	Areal density (kg/m ³)	Change in areal density
Bare		31.7	
2F		33.2	+ 4.7%
4F		34.7	+ 9.5%
2B		33.2	+ 4.7%
4B		34.7	+ 9.5%
2F2B		34.7	+ 9.5%

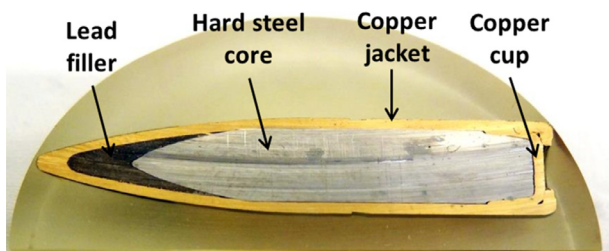


Fig. 1. Cross-section of the 7.62 × 63 M2 AP projectile used for the ballistic testing.

801 ± 6 m/s (\pm standard deviation). Projectile yaw and pitch was estimated by placing a yaw card 1.0 m in front of the target. Prior to conducting the testing of the targets, the measurements from the velocity screens, the yaw and pitch of the projectile, and subsequently the hole in the yaw card, were controlled by high speed filming. During the testing, the projectiles totally perforated the targets, and a cloud of debris, containing projectile and ceramic fragments, was formed at the backside of the targets.

Two sets of ballistic tests were performed; one with the aim of measuring the velocity of the core fragments after target perforation, and one with the aim of quantifying the fragmentation of the projectile core. The two slightly different experimental set-ups were employed since the fragments at the back of the target are best collected when the block of gelatine is positioned quite close to the backside of the target. First, for post-impact measurements to determine the residual velocity,

a high speed camera (FASTCAM SA-Z type 2100K, Photron) was used to measure the velocity of the largest fragment of the steel core. The frame rate was 80,000 fps and the resolution was 896×240 pixels. The camera was positioned orthogonally to the region behind the target. The region was lit by two sets of lamps (DS-3, Digital Sputnik). Also, a ruler was placed in this region below the path of the fragments. The ruler was used as a fixed point of reference for the distance travelled between consecutive frames. The recorded high speed videos were analysed using the software ImageJ [25] together with the software plugin MTrackJ [26] to find the velocity of the largest steel core fragment, the largest projectile jacket fragment and the front of the cloud of debris. The core and jacket velocity was measured roughly 0.4 m behind the ceramic tile where they were both clearly distinguished from the ceramic debris. The velocity of the ceramic cloud was measured approximately 0.1 m behind the ceramic tile. The number of tested targets of each type was four. In these tests, the block of gelatine shown in Fig. 2 was not employed. Second, for quantification of the fragmentation of the projectile steel core, blocks of ballistic gelatine were used as fragment catcher. The gelatine block was placed 0.2 m behind the target, and the area of the gelatine was then large enough to catch fragments from the cloud of debris coming from the target. Between eight and ten of these tests were conducted on each target type. This setup did not allow for an accurate measurement of the residual velocity from the high speed videos, since the target-gelatine distance was too short.

The ballistic test method employed here, broadly follows the method used by Carton and Roebroeks [27], and later employed by Burkins et al. [28]. Both studies employed the same 7.62×63 M2 AP projectile. However, those studies included all collected core fragments in the analysis of the kinetic energy-loss, while in the present study the mass of individual fragments are considered.

2.4. Fragment analysis

For fragment analysis after the ballistic testing, the gelatine that contained all the ceramic debris and the projectile fragments from the test was first dissolved in hot water. All fragments in the solution were then collected by filtering and drying. The fragments from the steel core are magnetic and they were separated from the other debris with the aid of a magnet.

The fragment size distribution of the retrieved core fragments was quantified by separating the fragments by size, employing a sieve shaker system (Vibratory Sieve Shaker ANALYSETTE 3, FRITSCH). Four sieve sizes were used; 4 mm, 2 mm, 1 mm and 0.5 mm. The sieve shaker was operating for a minimum of 6 min. The mass of the different fractions was then measured on a laboratory scale. The number of fragments in the size fractions > 4 mm and 2–4 mm were also counted.

Imaging of core fragments was performed using scanning electron microscopy (SEM) (SU6600 Schottky Field Emission Analytical SEM, Hitachi). The acceleration voltage was typically 3 kV, and the secondary electrons detector was employed to obtain the images.

3. Results

3.1. Ballistic testing

The target perforation process was filmed with a high speed camera, see Fig. 3, and the residual fragment velocity was measured from the video. It was observed that the projectile impact and perforation process results in significant fragmentation, not only of the projectile itself, but also of the ceramic in the targets. The high speed videos reveal that a cloud of fragments and other debris is formed at the backside of the target, as shown in the images in Fig. 3. The high hardness of the 7.62 mm M2 AP steel core means that fragmentation is expected for this projectile [29]. Close to the backside, the cloud is quite dense. However, at a distance of approximately 0.25 m, the individual fragments

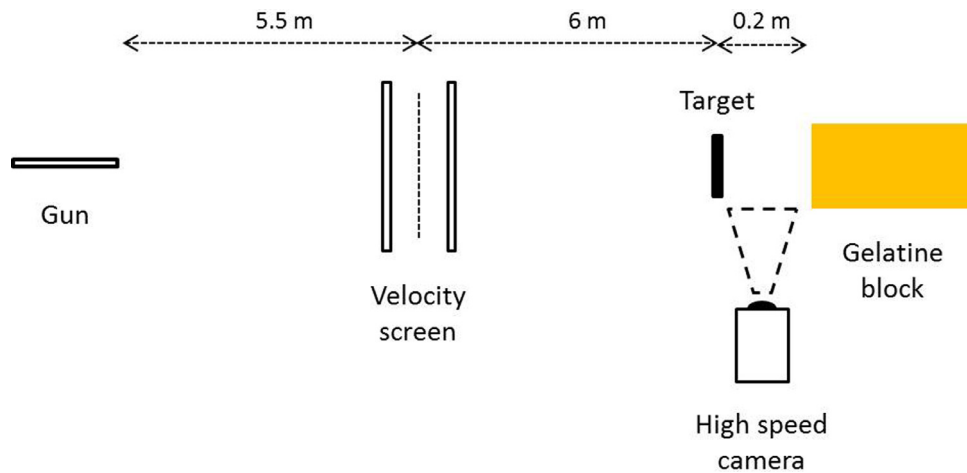


Fig. 2. Experimental setup for the ballistic testing.

(of some size) become clearly visible, see Fig. 3(c). The main reason for this is that the velocity of smaller and lighter fragments, particularly dust-like particles, are slowed down much faster than the larger fragments. In all the videos, the velocity of the largest fragment of the steel core could then be determined. This large fragment was almost exclusively in front of other smaller fragments inside the cloud, and in the cases where the residual velocity of the smaller core fragments could be measured, these travelled at a slightly lower velocity. There was no indication, however, that the velocity of the largest residual core fragment was decreased considerably within the length-range considered in these experiments. After recovery of the debris from the gelatine fragment catcher pieces of the projectile, i.e. core fragments and pieces of the copper jacket, as well as pieces from the target, were visible, see Fig. 4(a).

One observation from the high-speed videos was that the copper jacket of the projectile was always in front of the largest core fragment, as can be seen in Fig. 3(c–e). The experiments performed by Gooch et al. [30] may give some insight into these observations. By using X-ray imaging of the impact process between 7.62 mm M2 AP and boron carbide backed by polyethylene, they observed that the core started to decelerate before the jacket when the projectile impacted the ceramic. The jacket moved into the comminuted ceramic material while the core was still in the process of eroding. In the experiments by Gooch et al. [30], the projectile did not perforate the target. It is likely, however, that the observed behaviour, when combined with perforation, would have caused the jacket to perforate before the core and hence give a higher velocity after perforation, as was observed in the current study. It should be noted, however, that Burkins et al. [28] did not observe stripping of the jacket from the core in experiments where the projectile did actually perforate the target.

The ballistic impact had a similar effect on the fracture of the ceramic for the different types of targets. However, the amount of alumina that was still attached to the cover material after testing was very different, as shown in Fig. 4(b–c). For the back-covered targets, there was practically no alumina attached to the cover, i.e. there was complete delamination between the alumina and the composite cover. For the front-covered targets, however, approximately 150 g of alumina (of the original 318 g of alumina) was still attached to the cover, although with a very high scatter in alumina mass between the targets. Even more alumina, approximately 250 g, was left on the targets that were covered on both sides. Here, the scatter between the targets was very low, and on some targets both the front and back covers were still attached (this is not shown in Fig. 4). Also, the formation of radial cracks and cone cracks in the alumina in these targets, were observed.

3.2. Residual velocities

The measured velocities of the largest steel core fragment, the largest projectile jacket fragment, as well as the front of the debris cloud, are given in Table 2. The impact velocity was 801 ± 6 m/s (\pm standard deviation). For the largest core fragment, the residual velocity was between 513 ± 51 m/s and 571 ± 27 m/s (\pm 95% confidence limit), for target type 4B and target type 4F, respectively. However, none of these measurements clearly indicate that the target design, i.e. front and/or back composite cover on the alumina, has any effect on the residual velocity. Nevertheless, the velocity reduction of the steel core is high for each target type, and in the range 29–36%.

The measured residual velocities, V_{res} , from each experiment are shown in Fig. 5. In their experiments, Carton and Roebroeks [27] assumed that the residual fragment velocity was identical to the velocity of the front of the debris cloud measured from the high speed video. Also, Burkins et al. [28] combined X-ray measurements of the fragments inside the cloud and high speed videos of the front of the debris cloud. Their experiments confirmed the assumption by Carton and Roebroeks, since the difference in velocity between the two measurement methods was, in most cases, within 5%. However, when using high speed video to measure both the velocity of the front of the cloud and the largest core fragment inside the cloud, we found that the difference in velocity was in the range 7–14%, with an average of 10%. At the same time, the velocity of the largest jacket fragment was on average 5% lower than the initial cloud velocity. The point of measurement (0.1 m behind the target for the cloud velocity and 0.4 m behind for the jacket and the core velocity), may clearly affect this. However, these results show that the difference in velocity, despite differences in the point of measurement, could be significant, and that the possibility of this occurring is something that should be taken into account when using this test method. A large discrepancy between the results could contribute to inaccurate conclusions being made.

3.3. Core fragmentation

3.3.1. Fragments

The projectile steel core fragments were recovered after the ballistic tests with gelatine, and then separated by size. For all the targets, a few larger and many smaller fragments were created. The size distribution of the projectile core fragmentation is illustrated in Fig. 6, and more detailed images of core fragments are shown in Fig. 7. A similar type of fragmentation was observed by Savio et al. [31], although a different 7.62 mm AP projectile and a different ceramic were employed, with the tail piece of the steel core making up the largest fragment mass.

Images of core fragments are shown in Fig. 7. The SEM investigation

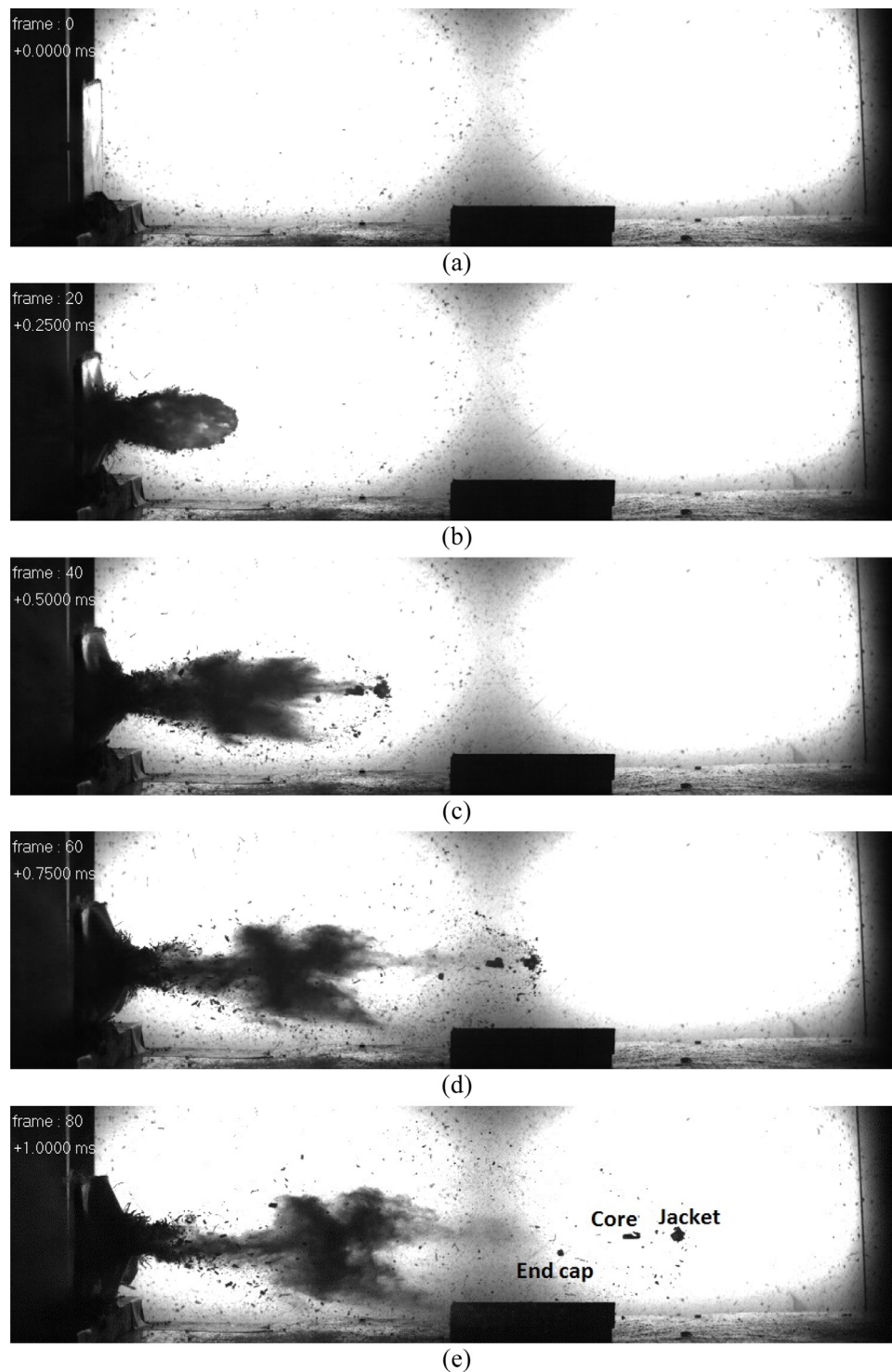


Fig. 3. Still images from the high speed video of target type 2F2B.

revealed the presence of micro-cracking close to the zone of projectile/alumina interaction. This observation, and the formation of the smaller fragments, is an indication of the high compressive forces that have been acting on the tip of the projectile core. An in-depth fractographic analysis has not been conducted as part of this study, but failure mechanisms such as inter-granular fracture, formation of adiabatic shear bands and ductile fracture have been identified for AP 7.62 mm hard steel core projectiles [13,32].

The majority of the small fragments, or particles, were 100 μm or larger in size, although fragments around 10 μm in size were also

observed. Particles of this small size have also been observed by Madhu et al. [33], which conducted impact experiments on alumina employing a 12.7 mm AP hardened steel projectile. They observed both projectile erosion and fragmentation, and higher impact velocity and higher ceramic thickness resulted in more erosion of the tip of the projectile, which was evident from the formation of a fine powder. In the present study, however, many of the smallest fragments may have been lost in the recovery process from the gelatine or in the handling of the samples. This may partly explain why around 10% of the initial core mass is unaccounted for (see next section) and why most fragments in the

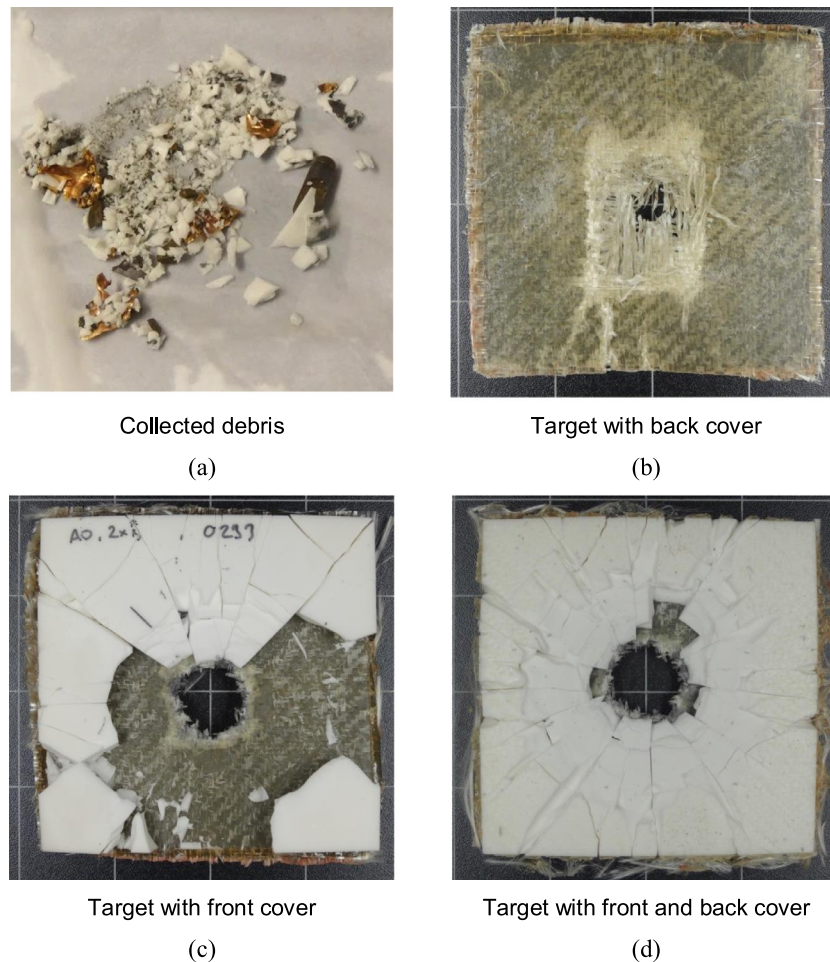


Fig. 4. Recovered debris and back face images of tested targets: (a) typical debris after filtering from the dissolved gelatine, (b) target with back cover (target type 2B), (c) target with front cover (target type 2F), and (d) target with front and back cover (target type 2F2B).

<0.5 mm size fraction were larger, not smaller, than 100 μm in size.

3.3.2. Mass of fragments

The results from the mass measurement of the different fragment sizes, after separation by sieves, are given in Table 2. Most of the residual mass was found in the largest size fraction, i.e. in the sieve with size 4 mm, including of course the largest core fragment. For the smaller size fractions, an increasingly lower residual mass is measured. This is also illustrated in Fig. 8, where the accumulated residual core mass, m_{res} , is shown (the figure is based on the data in Table 2). When taking smaller and smaller fragments into account, the accumulated core masses for the different target configurations become more and more similar, until around 90% of the initial core was recovered for all target types. This means that around 10% mass was lost in the impact process, some of this mass may have been lost on the front face of the target, and/or during the recovery of the fragments from the gelatine. There is no indication, however, that fragments of some significant size were lost, and it is likely that the lost mass is in the form of finer particles. It was also observed that some remnants of alumina were attached to the small fragments, but this is not enough to have any effect on the measured mass.

In general, the mass of the largest core fragment is on average about half of the initial core mass, m_0 , which is 5.19 g. The average residual mass of the largest core fragment was between 2.03 g and 3.04 g. It is noteworthy that the targets with the composite cover on the back side gave a lower residual mass of the largest fragment, compared to the targets with the composite cover on the front side. The difference between target type 4B (with back cover) on one hand, and target type 2F

(with front cover) on the other hand, was statistically significant, i.e. with the 95% confidence limit requirement that was employed, as illustrated in Fig. 9. The bare target, and the target with both back and front cover, gave a residual fragment mass that was in-between the mass for the targets with back or front cover. The mass reductions for target type 4F, the bare target, and target type 4B were 61%, 51%, and 43%, respectively. Taking all these results into account, there was a clear indication that the targets with the composite cover on the backside of the alumina gave a lower residual mass, m_{res} , of the largest core fragment.

The average mass of the largest fragment, and the remaining fragments that are larger than 4 mm in size, are shown in Fig. 9. The figure shows that a low mass of the largest fragment results in a comparatively high average mass of the smaller fragments, and vice versa. The number of fragments above 4 mm in size is also higher when the largest fragment has a low mass. Thus, these results show that a composite back cover results in formation of a higher number of smaller fragments (when considering the fragments above 4 mm in size). On average, the smaller fragments never have a mass that is higher than a typical 1.1 g fragment simulating projectile (FSP), as defined in STANAG 2920/AEP 2920 [23,24]. For the fragments that are below 4 mm in size, there is little variation between the different targets (see Table 2). However, the data for the size fraction 2–4 mm may also indicate that a back cover results in more core fragmentation, although the results are less clear for this size fraction. Overall, the results here show that a composite back cover on the alumina results in more fragmentation of the initial core, and ultimately gives a higher number of fragments of lower mass.

Table 2 Residual velocities from the ballistic testing, the mass of residual core fragment size fractions (the number of fragments in two size fractions is also given), and the residual velocity of the largest core fragment. All numbers given are average values \pm 95% confidence limits.

Target type	Residual velocity, V_{res} (m/s) (4 tests per sample type)				Residual mass, m_{res} (g) (8–10 tests per sample type)				Residual kinetic energy, E_{res} (J)			
	Largest core fragment	Largest jacket fragment	Front of debris cloud	Largest core fragment	> 4 mm, excl. largest	Fragment count (incl. largest)	2–4 mm	2–4 mm	Fragment count 2–4 mm	1–2 mm	0.5–1 mm	<0.5 mm
Bare	554 \pm 42	578 \pm 12	612 \pm 31	2.56 \pm 0.42	0.63 \pm 0.48	2.1 \pm 0.7	0.54 \pm 0.14	0.57 \pm 1.9	0.45	0.19	0.15	394 \pm 77
2F	528 \pm 18	577 \pm 5	611 \pm 13	3.04 \pm 0.33	0.19 \pm 0.22	1.3 \pm 0.3	0.62 \pm 0.29	6.3 \pm 1.9	0.40	0.20	0.15	423 \pm 50
4F	571 \pm 27	590 \pm 30	623 \pm 23	2.87 \pm 0.48	0.37 \pm 0.38	1.6 \pm 0.6	0.63 \pm 0.19	5.5 \pm 0.9	0.46	0.21	0.16	467 \pm 82
2B	553 \pm 45	574 \pm 19	595 \pm 17	2.36 \pm 0.39	0.58 \pm 0.31	2.1 \pm 0.6	0.82 \pm 0.22	7.1 \pm 1.8	0.43	0.25	0.19	361 \pm 73
4B	513 \pm 51	542 \pm 21	580 \pm 38	2.03 \pm 0.29	1.11 \pm 0.37	2.5 \pm 0.6	0.55 \pm 0.20	6.1 \pm 1.6	0.44	0.21	0.18	267 \pm 56
2F2B	520 \pm 35	557 \pm 23	577 \pm 29	2.43 \pm 0.54	0.30 \pm 0.41	1.5 \pm 0.6	0.84 \pm 0.26	9.0 \pm 2.7	0.52	0.26	0.19	329 \pm 78

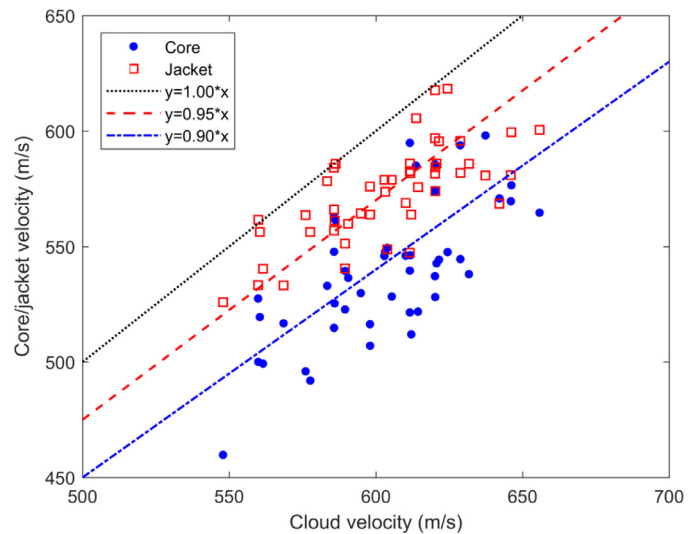


Fig. 5. The measured velocities of the largest core fragment, the largest jacket fragment and the front of the debris cloud. The three straight lines (with slopes of 1.00, 0.95 and 0.90) are visual guidelines for comparing the residual velocity of the projectile core and the jacket with the cloud velocity.

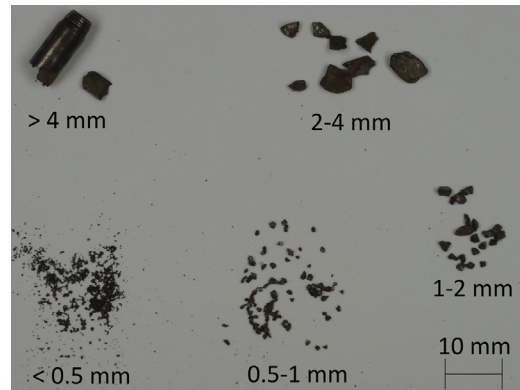


Fig. 6. Recovered projectile core fragments; example of size distribution.

3.4. Kinetic energy of residual core fragments

The kinetic energy of the core at impact is a function of the impact velocity, V_0 , and the initial core mass, m_0 . In the experiments conducted here, the kinetic energy of the core is then roughly 1665 J. Likewise, the residual kinetic energy of the largest projectile core fragment, E_{res} , can be calculated from the residual mass of the largest fragment, m_{res} , and the residual velocity, V_{res} , after target perforation. Here, only the largest fragment is considered in terms of residual kinetic energy, since it is by far dominant due to its high mass.

The residual kinetic energy, E_{res} , of the largest core fragment is given in Table 2. When comparing target type 4B (with back cover), the bare target and target type 4F (with front cover), the values of E_{res} for the largest core fragment are 267 ± 56 J, 394 ± 77 J and 467 ± 82 J, respectively. The kinetic energy-loss during impact on the target with a back cover is therefore higher, where the kinetic energy is reduced by up to 84% for target type 4B. The importance of the fragmentation of the core becomes evident when comparing target type 2B (with back cover) and target type 2F (with front cover). In this case, the largest fragment of the latter target actually had a slightly lower residual velocity; i.e. 553 ± 45 m/s for target type 2B and 528 ± 18 m/s for target type 2F. Still, due to a higher degree of core fragmentation, target type 2B with back cover had a lower kinetic energy of 361 ± 73 J, compared to the target with the front-cover, where the

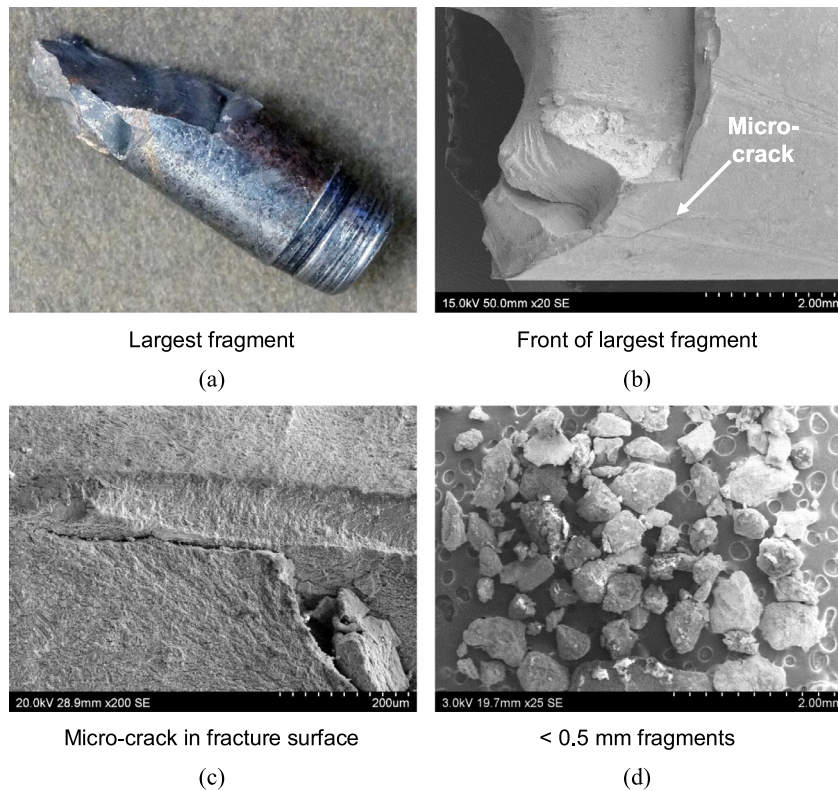


Fig. 7. Examples of core fragments: (a) Image of largest core fragment, tail section; and SEM images of (b) the front of a large fragment with a micro-crack on the side, (c) detail of a micro-crack in a fracture surface, and (d) fragments less than 0.5 mm in size.

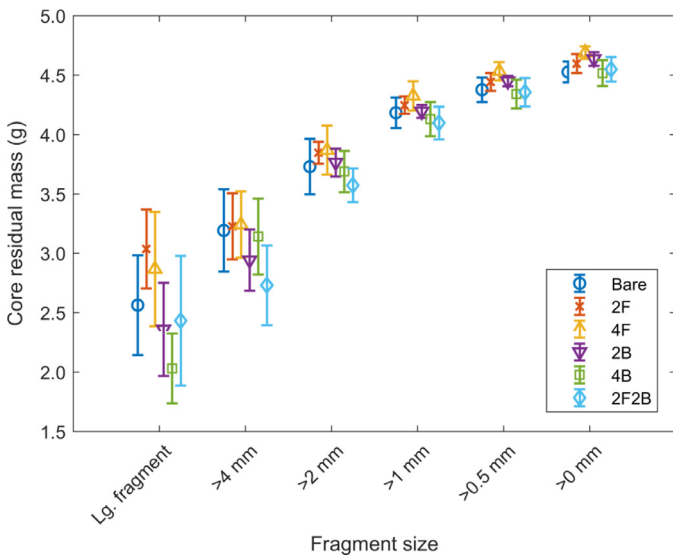


Fig. 8. Accumulated mass, m_{res} , of the residual core fragments including 95% confidence intervals.

kinetic energy was 423 ± 50 J. It should not be neglected, however, that a fragment cloud will have a higher total kinetic energy, and therefore potentially represent a higher threat. Still, the contribution from the largest fragment is by far the dominant in this case.

The relative residual mass, m_{res}/m_0 , and the relative residual velocity, V_{res}/V_0 , for the largest core fragment that was recovered from each target type, is shown in Fig. 10. In this figure, the points closer to the lower left corner in the figure indicate lower kinetic energy, while the points that are closer to the upper right corner indicate higher kinetic energy. As when considering only the mass of the largest fragment, the

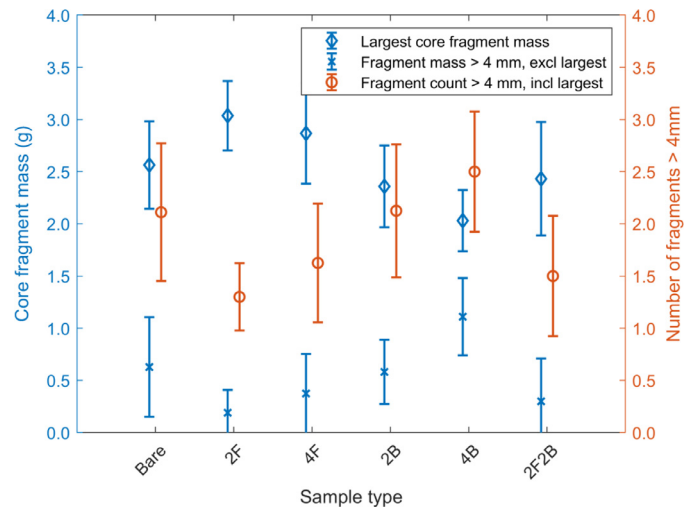


Fig. 9. Average mass of the largest core fragment and the average mass of the remaining fragments larger than 4 mm in size. The average number of fragments larger than 4 mm in size, including the largest fragment, is also indicated. The bars indicate the 95% confidence intervals.

figure indicates that the residual kinetic energy, E_{res} , of the largest core fragment can be reduced by adding a composite back cover to the alumina. However, although the results in Fig. 10 indicate that there the kinetic energy-loss of the projectile steel core is higher when a composite back cover is added to the alumina, this cannot be confidently concluded. This is due to the large and overlapping confidence intervals.

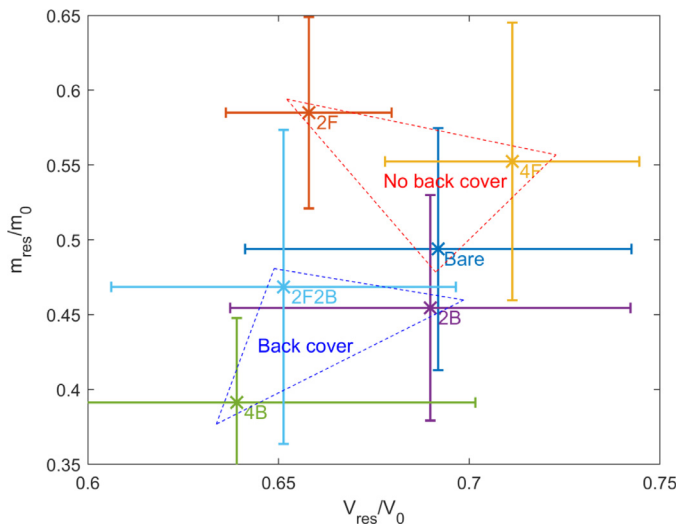


Fig. 10. Relative residual mass, m_{res}/m_0 , and relative residual velocity, V_{res}/V_0 , for the largest core fragments. The bars indicate the 95% confidence intervals. The red dashed triangle shows the three targets with no back cover, while the blue dashed triangle includes the three targets with back cover. (For interpretation of the references to color in this figure legend, the reader is referred to the web version of this article.)

4. Discussion

There are some studies in the literature that look into the effects on ballistic performance of adding a composite cover to ceramics. An overview of some of this literature is given in Table 3. Several of the studies have shown that covering of ceramics may lead to improved ballistic performance in terms of increased core fragmentation, reduced residual velocity of the core fragments, and increased kinetic energy-loss. However, all these studies differ from each other in that the tested targets, the test methods and the projectiles are different. It is therefore difficult to directly compare the results. One common observation, however, is that most studies found a significant effect from a front cover or from wrapping of the ceramic. That is different from the results of the current study, which indicate that the greatest improvement in ballistic performance is found when adding a back cover. No other studies have, to our knowledge, reported a similar effect, although increased energy absorption from a back cover has been reported for very thin (2 mm) alumina tiles [18].

In one of the studies, Sarva et al. [14] found a significant improvement in the ballistic performance from front covers made of different materials. Significantly higher kinetic energy-loss and more projectile erosion (i.e. damage) were observed. The increase in performance was attributed to an increased flow of ceramic debris towards the projectile due to constraints from the front cover, and the addition of an additional back cover had only a very modest effect. However, Sarva et al. [14] employed a cylindrical flat-ended tungsten heavy alloy (WHA) penetrator (which was of similar mass as the 7.62 mm M2 AP projectile) in their impact experiments. The WHA penetrator was continuously consumed by erosion by the penetration, and did not shatter or break, which reduced the scatter in the data. This is different from projectiles made of hard steel, such as e.g. the 7.62 mm M2 AP, which have been observed to fragment during impact due to their low ductility [16,29–33]. It has been shown that the perforation ability of AP projectiles can be directly correlated with the hardness of the core material [13]. Less hard projectiles, on the other hand, will result in other deformation modes, such as e.g. mushrooming or petalling. It has also been observed that a composite cover did not have a significant effect on the erosion of a mild steel core projectile [19]. Nevertheless, the different degradation processes of the penetrator could at least partly explain the difference observed in the current study and the one

Table 3
Experimental work in the literature that discuss the effect of adding a composite cover to ceramic tiles.

Reference	Projectile	Impact conditions	Ceramic	Cover material	Target design	Main conclusions on effect of cover
Numm et al. [15]	7.62 mm AP M61	V50 (625–878 m/s)	6.2 mm PAD B ₄ C	UD carbon fibre/epoxy, PBO/vinylester	Front and back cover, 2–8 layers on each side, 1 mm spall cover and 7.25 mm backing of UHMWPE	Penetration resistance increases with increasing number of plies
Sarva et al. [14]	6 mm tungsten heavy alloy (WHA), cylindrical flat-ended, mass 10.68 g	~900 m/s	12.7 mm 99.5% Al ₂ O ₃ , 12.7 mm SiC	UD glass fibre tape, E-glass/epoxy weave, carbon fibre/epoxy weave, Ti-alloy sheet	Mainly front cover, 1–9 composite layers, Ti-alloy thickness 0.127–0.762 mm	Front-face restraint gives reduction in projectile kinetic energy, mass and velocity
Reddy et al. [16]	7.62 mm AP projectile, mass 10.44 g, 5.2 g hardened steel core	820 ± 10 m/s	7 mm 99.5% Al ₂ O ₃	UD UHMWPE, aramid fabric	Wrapping in 2–4 layers, i.e. 2–4 layers on each side, backed by 10 mm E-glass laminate	Higher energy absorption, lower projectile residual mass and velocity with increasing number of wrapping layers
Crouch [20]	7.62 mm M2 AP	868–887 m/s, multi-hit	9 mm SiC	Elastomeric film, polyester or polypropylene fibre/epoxy, aramid fibre/epoxy	Hard armour plates with clad ceramic, UHMWPE backing and nylon fabric wrap	Increase in number of radial ceramic cracks, and decrease in back-face deformation with fibre-reinforced cover
Crouch et al. [19]	7.62 mm AK-47, mass 7.91 g, 3.59 g mild steel core	697–739 m/s, reverse ballistics	3, 4 and 5 mm B ₄ C	Aramid fibre/epoxy	Front and back cover, with or without 30 ply UHMWPE backing, some targets with air gap between backing and sabot	Little effect on projectile deformation and erosion
Öberg et al. [18]	8 mm spherical projectile, 52.100 type steel, mass ~2 g	220–230 m/s	2 mm Al ₂ O ₃	Carbon fibre/PET weave	1 layer back cover	Higher energy absorption from back cover
Rahbek et al. [17]	7.62 mm AP M61, 3.7 g hardened steel core	176–351 m/s	10 mm 98% Al ₂ O ₃	Glass fibre/PET fabric	Front and back cover, 2 layers on each side	Increased ceramic damage, no difference in projectile core damage

by Sarva et al. [14].

In addition to the penetrator material, the penetrator shape will also have an effect, meaning that a different shape of the nose of the projectile may lead to different penetration mechanisms and perforation velocities [34,35]. Conical or ogival tipped projectiles may penetrate at lower velocities than cylindrical/blunt projectiles. This may also explain some of the observed differences between the current study and that by Sarva et al. [14]. The increased flow of ceramic debris against the projectile due to constraints from the front cover may not be as significant for pointed projectiles. In fact, the front-covered alumina did not result in lower residual mass than the bare targets which suggests that this mechanism is negligible for the target/penetrator combination that was employed here. To complicate things further, the same projectile core with and without the jacket and lead cap can also have very different penetration ability [19,30]. Still, noteworthy effects of a composite front cover or wrapping on ceramic damage, core erosion, fragmentation, and back-face deformation, have been observed also for pointed AP 7.62 mm projectiles of hardened steel by Nunn et al. [15], Reddy et al. [16] and Crouch [20]. The suggested mechanisms that contribute to the improved performance are quite similar to those proposed by Sarva et al. [14]. The constraint of the ceramic could slow down the opening of cracks, giving more ceramic damage and ceramic debris of smaller size in the region in front of the penetrator. The ceramic then takes part in the loading and erosion of the penetrator for a longer period of time. These mechanisms do, however, not fully explain the improvement in ballistic performance from a back cover only. In the case of a back cover, it is more likely that the composite restraint contributes to a delayed opening of tensile cracks on the back of the ceramic. The end result is similar though, since the delay in separation of larger ceramic pieces created by cone and radial cracks gives more time for interaction with the penetrator. Hence, in the present study, increased core fragmentation and higher energy-loss are observed for the targets with a back cover.

In the targets tested here, the areal density was increased by 4.7% and 9.5% when two or four layers, respectively, of cover material was added to the alumina. The increased areal density of the covered targets will contribute to the increased ballistic performance, and it has been argued that the dwell time for a ceramic/composite system will increase with increasing areal density, as long as the ceramic is harder than the penetrator [36]. However, a small increase in areal density is, on its own, not able to explain the observed effects on core fragmentation, residual velocity and kinetic energy-loss. Similar observations were also made in the other studies discussed above, where an up to 50% change in energy-loss, residual velocity, fragmentation and V50 (projectile velocity at which the chance of perforation is 50% with a specified armour and a specified projectile) were observed for less, sometimes much less, than a 10% increase in areal density [14–16]. This supports the presumption that some supplementary mechanisms, as discussed above, must be acting and contributing to the observed effects.

Improved ballistic performance of the covered or wrapped ceramic tile in hard armour plates in body armour could have implications on the overall weight of the soldier protection system. There are several possible outcomes of increased core fragmentation and perforation resistance. One is that the thickness of the ceramic itself could be reduced, while still maintaining the required level of protection at a lower areal density. Another is that the number of sheets of ballistic fibres, either at the back of the hard armour plate or in the soft ballistic panel, could be reduced. This is a direct consequence of the lower kinetic energy of the core fragments. Also, improved multi-hit performance may result, since the composite restraint can prevent through-thickness cracks from opening, as well as confine larger ceramic fragments. With an optimised design of the composite that is surrounding the ceramic tile, seen in conjunction with the whole protection system, the mobility of the soldier could be improved at a reasonable cost. An alternative, however, is to build systems that exhibit higher performance and protect against more severe threats.

From the results presented here, it was difficult to draw any firm conclusions, although some clear trends were observed. One important factor to consider in this respect is that the data are generated from, in a statistics point of view, only a limited number of tests for each target type. In total, 75 tests were performed for the results shown in this study. The number of tests should have been much higher to achieve statistically reliable results at a high confidence level. The reason for the limited number of conducted tests is that the test methods that were employed, e.g. using gelatine as a fragment catcher, are very time-consuming and expensive.

5. Conclusions

Ballistic experiments have been performed on bare and composite-covered alumina tiles. The main aim of the experiments was to isolate the possible differences in ballistic performance when adding front or back covers on ceramic tiles. Two or four layers of a glass fibre-reinforced composite material were applied to the front and/or backside of the alumina, which resulted in a maximum increase in areal density of 9.5%.

In the ballistic experiments, free-standing targets with different alumina/composite configurations were totally perforated by a 7.62 mm AP hard steel core projectile at near-muzzle velocities. The perforation process was monitored by high speed video, and the residual core fragments were collected and analysed. This allowed the effect of the projectile/target interaction to be quantified in terms of the residual size of the core fragments. It was observed that the target configuration had a significant influence on the fragmentation of the projectile core. The targets with the composite cover on the back side gave higher core fragmentation, i.e. a higher number of fragments above 4 mm in size were formed, and the residual mass of the largest fragment was lower. A reduction of the core mass by 61% was observed for the targets with four composite cover-layers on the back of the alumina.

The position of the composite cover did not have a significant effect on the residual velocity of the main core fragment after target perforation. However, due to the difference in residual mass, the kinetic energy-loss was higher when a back cover was applied. A reduction in kinetic energy by 84% (for the largest fragment) was achieved with four composite cover-layers on the back of the alumina. The observed effects are somewhat different from several studies in the literature, where an improvement in ballistic performance has been attributed to composite covering on the front side of the ceramic, i.e. on the strike face, or by wrapping of the ceramic by the composite.

The increased areal density alone cannot explain the increased fragmentation of the projectile core, and some other mechanisms must also contribute. The most likely mechanism is that the restraint of the back cover contributes to a time-delay in the opening of tensile cracks on the back of the ceramic. This delay gives more time for interaction with the penetrator, hence improving the ballistic performance of the target.

Acknowledgements

The authors would like to acknowledge Lasse Sundem-Eriksen, Ole Andreas Haugland and Torbjørn Olsen (FFI) for their contribution to this work.

References

- [1] Hazell PJ. *Ceramic armour: design and defeat mechanisms*. Canberra, Australia: Argos Press; 2006.
- [2] Zaera R. Ballistic impacts on polymer matrix Composites, composite armor, personal armor. In: Abrate S, editor. *Impact engineering of composite structures*. 526th ed. Vienna: Springer; 2011. p. 305–403.
- [3] Washington, D.C., USA: The National Academies Press; 2011.
- [4] Shockey DA, Simons JW, Curran DR. *The damage mechanism route to better armor*

- materials. *Int J Appl Ceram Technol* 2010;7(5):566–73.
- [5] Compton BG, Gamble EA, Zok FW. Failure initiation during impact of metal spheres onto ceramic targets. *Int J Impact Eng* May 2013;55(0):11–23.
- [6] Wilkins ML, Cline CF, Honodel CA. Fourth progress report of light armor program. Livermore, California, USA: Lawrence Radiation Laboratory, University of California; Feb. 1969. UCRL-50694.
- [7] Shockey DA, Marchand AH, Skaggs SR, Cort GE, Burkett MW, Parker R. Failure phenomenology of confined ceramic targets and impacting rods. *Int J Impact Eng* 1990;9(3):263–75.
- [8] LaSalvia JC, McCauley JW. Inelastic deformation mechanisms and damage in structural ceramics subjected to high-velocity impact. *Int J Appl Ceram Technol* 2010;7(5):595–605.
- [9] Sherman D, Ben-Shushan T. Quasi-static impact damage in confined ceramic tiles. *Int J Impact Eng* 1998;21(4):245–65.
- [10] Owens BD, Kragh JF, Wenke JC, Macaitis J, Wade CE, Holcomb JB. Combat wounds in operation Iraqi freedom and operation enduring freedom. *J Trauma-Injury Infect Crit Care* 2008;64(2):295–9.
- [11] Medvedovski E. Ballistic performance of armour ceramics: influence of design and structure. Part 2. *Ceram Int* 2010;36(7):2117–27.
- [12] Horsfall I, Buckley D. The effect of through-thickness cracks on the ballistic performance of ceramic armour systems. *Int J Impact Eng* 1996;18(3):309–18.
- [13] Di Benedetto G, Matteis P, Scavino G. Impact behavior and ballistic efficiency of armor-piercing projectiles with tool steel cores. *Int J Impact Eng* 2018;115:10–8.
- [14] Sarva S, Nemat-Nasser S, Mcgee J, Isaacs J. The effect of thin membrane restraint on the ballistic performance of armor grade ceramic tiles. *Int J Impact Eng* 2007;34(2):277–302.
- [15] Nunn SD, Hansen JGR, Frame BJ, Lowden RA. Improved ballistic performance by using a polymer matrix composite facing on boron carbide armor tiles. In: Swab JJ, editor. *Advances in ceramic armor*. The American Ceramic Society; 2005. p. 287–92.
- [16] Reddy P, Madhu V, Ramanjaneyulu K, Bhat T, Jayaraman K, Gupta N. Influence of polymer restraint on ballistic performance of alumina ceramic tiles. *Def Sci J* 2008;58(2):264–74.
- [17] Rahbek DB, Simons JW, Johnsen BB, Kobayashi T, Shockey DA. Effect of composite covering on ballistic fracture damage development in ceramic plates. *Int J Impact Eng* Jan. 2017;99:58–68.
- [18] Oberg EK, Dean J, Clyne TW. Effect of inter-layer toughness in ballistic protection systems on absorption of projectile energy. *Int J Impact Eng* Feb. 2015;76(0):75–82.
- [19] Crouch IG, Appleby-Thomas G, Hazell PJ. A study of the penetration behaviour of mild-steel-cored ammunition against boron carbide ceramic armours. *Int J Impact Eng* Jun. 2015;80:203–11.
- [20] Crouch IG. Effects of cladding ceramic and its influence on ballistic. 28th international symposium on ballistics. 1 and 2. 2014. p. 1084–94.
- [21] Lausund KB, Johnsen BB, Rahbek DB, Hansen FK. Surface treatment of alumina ceramic for improved adhesion to a glass fibre-reinforced polyester composite. *Int J Adhes Adhes* Dec. 2015;63:34–45.
- [22] Børvik T, Dey S, Clausen AH. Perforation resistance of five different high-strength steel plates subjected to small-arms projectiles. *Int J Impact Eng* 2009;36(7):948–64.
- [23] STANAG 2920 (Edition 3) - Classification of Personal Armor. Brussels, Belgium: Nato Standardization Agency (NSA); 2014.
- [24] AEP-2920: Edition A - Procedures for the evaluation and classification of personal armour - Bullet and fragmentation threats. Nato Standardization Agency (NSA); 2014.
- [25] Schneider CA, Rasband WS, Eliceiri KW. NIH image to ImageJ: 25 years of image analysis. *Nat. Methods* Jun. 2012;9:671.
- [26] Meijering E, Dzyubachyk O, Smal I. Chapter nine - Methods for cell and particle tracking. In: conn PM, editor. *Methods in enzymology imaging and spectroscopic analysis of living cells*. 504th ed. Academic Press; 2012. p. 183–200.
- [27] Carton E, Roebroeks G. Testing method for ceramic armor and bare ceramic tiles. 38th international conference and exposition on advanced ceramics and composites. Jan. 2014. p. 26–31.
- [28] Burkins MS, Little DJ, Love MS. A potential methodology for evaluating ceramic quality. 30th international symposium on ballistics. Sep. 2017. p. 11–5.
- [29] Rakvag KG, Børvik T, Westermann I, Hopperstad OS. An experimental study on the deformation and fracture modes of steel projectiles during impact. *Mater Des* 2013;51:242–56.
- [30] Gooch WA, Burkins MS, Hauver G, Netherwood P, Benck R. Dynamic X-ray imaging of the penetration of boron carbide. *J Phys IV* 2000;10(P9):583–8.
- [31] Savio SG, Ramanjaneyulu K, Madhu V, Bhat TB. An experimental study on ballistic performance of boron carbide tiles. *Int J Impact Eng* Jul. 2011;38(7):535–41.
- [32] Savio SG, Senthil P, Singh V, Ghoshal P, Madhu V, Gogia AK. An experimental study on the projectile defeat mechanism of hard steel projectile against boron carbide tiles. *Int J Impact Eng* Dec. 2015;86:157–66.
- [33] Madhu V, Ramanjaneyulu K, Balakrishna Bhat T, Gupta NK. An experimental study of penetration resistance of ceramic armour subjected to projectile impact. *Int J Impact Eng* Dec. 2005;32(1–4):337–50.
- [34] Lundberg P, Renstrom R, Lundberg B. Impact of conical tungsten projectiles on flat silicon carbide targets: transition from interface defeat to penetration. *Int J Impact Eng* 2006;32(11):1842–56.
- [35] Dey S, Børvik T, Hopperstad OS, Leinum JR, Langseth M. The effect of target strength on the perforation of steel plates using three different projectile nose shapes. *Int J Impact Eng* 2004;30(8):1005–38.
- [36] Carton E, Roebroeks G, Weerheijm J, Diederer A, Kwint M. TNO's research on ceramic based armor. 39th international conference and exposition on advanced ceramics and composites. Jan. 2015. p. 25–30.